ACS chemical biology

pubs.acs.org/acschemicalbiology

Articles

Allosteric Inhibition of Parkinson's-Linked LRRK2 by Constrained Peptides

Leah G. Helton,[%] Ahmed Soliman,[%] Felix von Zweydorf, Michalis Kentros, Jascha T. Manschwetus, Scotty Hall, Bernd Gilsbach, Franz Y. Ho, Panagiotis S. Athanasopoulos, Ranjan K. Singh, Timothy J. LeClair, Wim Versées, Francesco Raimondi, Friedrich W. Herberg, Christian Johannes Gloeckner, Hardy Rideout, Arjan Kortholt,* and Eileen J. Kennedy*

Cite This: *ACS Chem. Biol.* 2021, 16, 2326−2338

Read Online

ACCESS | Metrics & More | Article Recommendations | Supporting Information

ABSTRACT: Leucine-Rich Repeat Kinase 2 (LRRK2) is a large, multidomain protein with dual kinase and GTPase function that is commonly mutated in both familial and idiopathic Parkinson's Disease (PD). While dimerization of LRRK2 is commonly detected in PD models, it remains unclear whether inhibition of dimerization can regulate catalytic activity and pathogenesis. Here, we show constrained peptides that are cell-penetrant, bind LRRK2, and inhibit LRRK2 activation by downregulating dimerization. We further show that inhibited dimerization decreases kinase activity and inhibits ROS production and PD-linked apoptosis in primary cortical neurons. While many ATP-competitive LRRK2 inhibitors induce toxicity and mislocalization of the protein in cells, these constrained peptides were found to not affect LRRK2 localization. The ability of these peptides to inhibit pathogenic LRRK2 kinase activity suggests that disruption of dimerization may serve as a new allosteric strategy to downregulate PD-related signaling pathways.

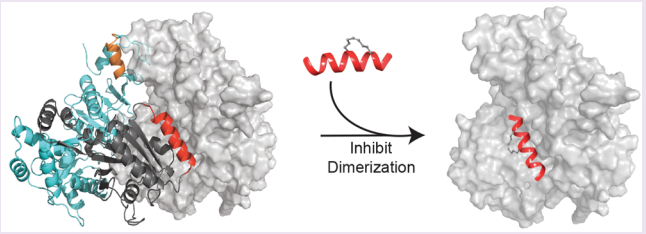

INTRODUCTION

Parkinson's Disease (PD) is the second most common neurodegenerative disorder worldwide, with over 10 million active cases globally and at least 60 000 new diagnoses in the US each year.[1] PD can result in bradykinesia, resting tremor, postural instability, rigidity, and memory loss, with the severity of the disease varying among individuals.[2] While aging remains the largest risk factor for PD, the relatively recent identification of over 20 genes associated with familial PD highlights potential signaling pathways involved in disease pathogenesis.[3−8] Despite only 5−10% of PD cases exhibiting a genetic basis, identifying pathways altered in the genetic form of the disease could provide insight into innovative therapeutic targets and treatment strategies.[9]

Missense mutations in Leucine-Rich Repeat Kinase 2 (LRRK2) are the most common cause of genetic PD and are also present in a significant portion of idiopathic PD (iPD) cases.[10] LRRK2 mutations are relatively common, accounting for 5−6% of familial PD cases and 1−2% of sporadic PD cases; this prevalence is significantly larger in specific ethnic groups.[11] Containing an armadillo domain (ARM), an ankyrin repeat (ANK), a leucine-rich repeat (LRR), a Ras-like GTPase (RocCOR) domain, a Ser/Thr kinase domain, and a C-terminal WD40 domain, the large 2527 amino acid structure and complex activation mechanism of LRRK2 have incited investigation into the underlying mechanism(s) driving its pathogenesis.[12,13] PD-associated LRRK2 mutations are most abundant in the catalytic core of the protein: the RocCOR GTPase domain (R1437H, R1441G/H/C, Y1699C) and the protein kinase domain (G2019S, I2020T).[14] Each mutation results in altered GTPase and/or kinase activity, and this aberrant activity triggers alterations in vesicular trafficking, cytoskeletal dynamics, autophagy, lysosomal function, oxidative stress, neurotransmission, and mitochondrial function.[15] Importantly, a common noncoding variation in *LRRK2* modulates risk for PD.[16] Moreover, elevated LRRK2 kinase activity, independent of mutations, was even reported in iPD,[17] indicating that targeting LRRK2 is not only beneficial for the population who carry pathogenic *LRRK2* coding variants but might also be relevant for iPD patients carrying a wild-type version of this gene.

Successful inhibition of the kinase domain of LRRK2 using ATP-competitive small molecule inhibitors leads to downregulated kinase activity, reduced oxidative stress, and limited neuronal toxicity.[18] However, a major shortcoming of these small molecule inhibitors is that they also induce mislocaliza-

Received: June 25, 2021
Accepted: August 25, 2021
Published: September 8, 2021

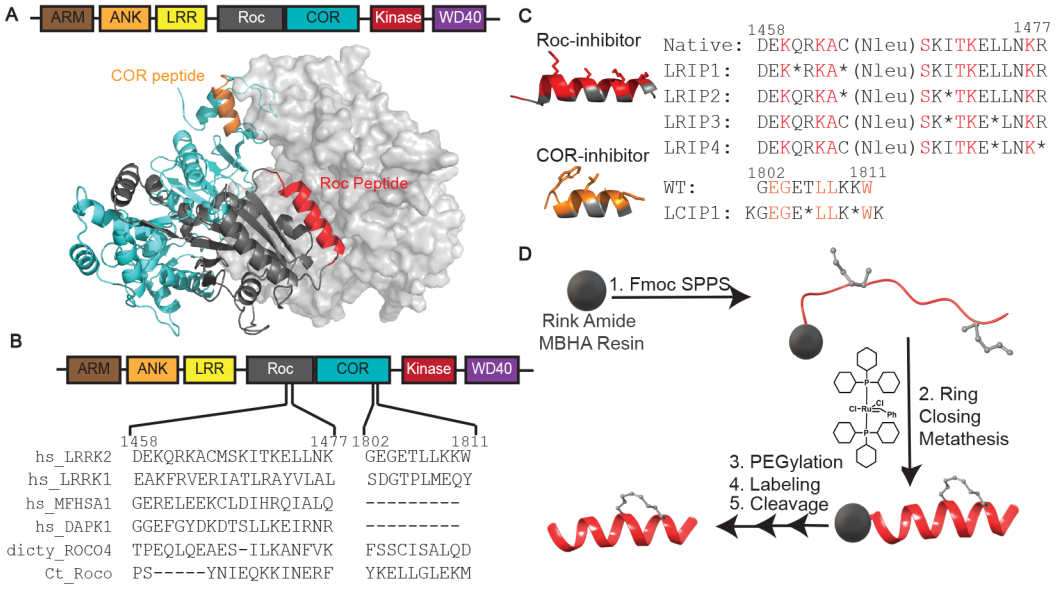

Figure 1. Design and synthesis of stapled peptide dimerization disruptors of LRRK2. (a) Domain architecture of LRRK2 and homology model of the RocCOR dimer interface. The Roc domain is shown in dark gray, and the COR domain is shown in cyan. The Roc peptide is highlighted in red, and the COR peptide is highlighted in orange. The dimer interface is indicated by the light gray surface. (b) Sequence alignments of LRRK2 to other Roco proteins at the indicated interfaces. (c) Peptide library sequences were designed to preserve amino acids at the predicted interface (red/orange). Non-natural amino acids were substituted on the predicted nonbinding interface (gray). (d) Schematic of Fmoc-based Solid Phase Peptide Synthesis (SPPS) and ring-closing metathesis.

tion of LRRK2, resulting in altered vesicular trafficking and lysosomal function, mitochondrial dysfunction, and lung and kidney abnormalities.[17,19] Therefore, this has severely limited the translational potential of currently available small molecule inhibitors of LRRK2 and underscores the need for alternative targeting strategies to inhibit LRRK2 function. One possible strategy would be to take advantage of the different states of LRRK2 cycles between, as part of the regulation of its kinase function. Structural and functional assays have shown LRRK2 cycles between the cytoplasm and membranous organelles.[20−22] In the cytosol, LRRK2 appears to be mostly monomeric and has low kinase activity, while it is predominantly dimeric and active when localized at membranes. Furthermore, several LRRK2 PD variants result in an impaired monomer−dimer equilibrium. These data thus suggest that dimer formation and kinase activation are directly linked.[20−26] Furthermore, recent structural work[27−29] and molecular dynamics simulations[30] indicate that changes in the kinase domain allosterically signal back and forth throughout the entire molecule.[31] This could potentially be exploited as an effective strategy for allosteric inhibition of LRRK2 kinase activity.

In order to analyze the role of LRRK2 dimerization on kinase regulation, we designed peptides modified to contain an all-hydrocarbon constrained macrocycle to serve as protein−protein interface (PPI) disruptors to block the dimer interface. In contrast to small molecule inhibitors, which rely on hydrophobic pockets and the engagement of a few key amino acids for binding, peptides can target elongated binding surfaces that are typically ill-suited to small molecules.[32] Incorporation of the hydrocarbon staple into the desired peptide sequence was done as a strategy to create cell-permeable peptides. The design and synthesis of peptides to effectively disrupt protein−protein interactions has been applied to a diverse array of targets across multiple diseases (for example, see refs 33−38). Here, we developed constrained peptides designed to target the LRRK2 RocCOR dimerization interface. These peptides permeate cells, bind to LRRK2, and reduce kinase activity and reactive oxygen species (ROS) production. Furthermore, the peptides reduce the toxic cellular effects seen with pathogenic LRRK2 in primary cortical neurons. Additionally, the allosteric inhibitors do not appear to induce mislocalization of LRRK2 to the microtubules that is frequently seen with small molecule inhibitors. This work supports the hypothesis that dimerization is an important regulator of kinase activity, and dimerization disruption may serve as a new therapeutic strategy for the treatment of LRRK2-mediated PD pathogenesis.

RESULTS AND DISCUSSION

Design of Stapled Peptides Targeting the RocCOR Dimerization Interface of LRRK2. Until recently (see refs 27−29), purification and structure elucidation of LRRK2 constructs have proven elusive, in large part due to the large, complex nature of the protein; therefore, structural studies have initially focused on characterization of bacterial homologs, namely, "Roco" proteins.[39,40] As the RocCOR GTPase domain is considered essential for mediating LRRK2 dimerization,[41−43] we analyzed a structural model of this dimer interface to identify components of the interface that may contribute to dimer formation.[44] We identified two key sequences, one in the Roc domain and one in the COR domain, that appear to contribute to the dimerization interface by binding along large hydrophobic clefts [Figure 1A]. Newly released cryoEM structures[28,29] confirm the helical nature of LRIP, but the contribution of this helix to the dimer interface is unclear. Differences in these structures depending on activation state of LRRK2 reveal that the Roc and COR domains may adopt multiple conformations, and the Roc inhibitors may interfere with the dimer interface in either a

https://doi.org/10.1021/acschembio.1c00487
ACS Chem. Biol. 2021, 16, 2326−2338

direct or an indirect manner as LRRK2 transitions between inactive and active conformers. Sequence alignment of these peptide sequences across the family of human Roco proteins indicates that these sequences in the protein−protein interface are unique to LRRK2 [Figure 1B]. From this model, we sought to determine which amino acids may be essential for dimer formation. After analyzing the sequence, homologous protein structures,[40] and the structural model of LRRK2,[44] amino acids that were predicted to be involved in mediating the protein−protein interaction (PPI) were identified [Figure 1C, red and orange]. Peptides were derived from these regions where the amino acids predicted to comprise the PPI remained unchanged while olefinic amino acids were introduced in positions that were not predicted to contribute to dimerization [Figure 1C, black]. The olefinic amino acid Fmoc-(S)-2-(4-pentenyl)alanine was incorporated at *i*, *i*+4 positions along the nonbinding interface[45] to form hydrocarbon macrocycles with the intent to improve cell permeability as compared to the native, unmodified peptide sequence. In addition, we designed a small library of Roc domain-derived peptides with shifted stapled positions to identify the ideal position for minimal interference with target binding. The COR-targeting peptide was much shorter, so olefinic amino acids were incorporated at the only *i*, *i*+4 positions that were suitable for replacement [Figure 1C]. Peptides were synthesized using Fmoc-based solid phase peptide synthesis (SPPS) on solid support, and the olefinic amino acids were cyclized using Grubbs I Catalyst while on solid support to yield the constrained peptide products [Figure 1D]. Further modification included incorporation of an N-terminal PEG_3 linker to improve hydrophilicity of the peptide and additional N-terminal labeling with either biotin or 5,6-carboxyfluorescein (FAM) for biochemical and cellular assays. Recently released structures[28,29] identified the LCIP1 sequence as being predominantly nonhelical; therefore, we performed circular dichroism and determined that LCIP1 is not in a purely helical or beta-sheet conformation but instead adopts a mixture of different secondary structural elements [Figure S1].

LCIP1 and LRIP4 Bind to LRRK2. Peptides designed to target the Roc domain (LRRK2 Roc Interacting Peptides, LRIP) and COR domain (LRRK2 COR Interacting Peptides, LCIP) were first passed through a preliminary screen to determine whether they had any inhibitory effects LRRK2 dimerization [Figure S2] by assessing coimmunoprecipitation of differently tagged LRRK2 constructs. From this screen, LRIP3, LRIP4, and LCIP1 appeared to partly downregulate dimerization. The peptide libraries were also screened by fluorescence polarization (FP) to determine whether they bound their target domains of LRRK2 [Figures 2A,B and S3]. Two MBP-tagged protein constructs, COR and RocCOR, were purified and plated in concentrations ranging from 5 μM to 1 nM along with 10 nM FAM-labeled peptides. While most of the peptides demonstrated no appreciable binding curves to these protein constructs, LRIP4 exhibited a binding affinity in the mid-nanomolar range (~60 nM) while LCIP1 bound to the CORB construct with significantly weaker interaction in the low micromolar range (~1 μM; Figures 2A,B and S3). The weak binding of LCIP1 to its target domain may be due, at least in part, to its secondary structural conformation, which differs from that in the newly released full-length structure of LRRK2. To ensure that the detectable binding by the lead peptides, LRIP4 and LCIP1, was toward their target domain and not the MBP tag, FP assays were performed with MBP alone. Both peptides exhibited no binding to this construct [Figure S4], indicating that they appear to bind their targeted domains in LRRK2.

A

Compound	MBP-RocCOR
LRIP Native	n.d.[1]
LRIP 1	n.d.
LRIP 2	n.d.
LRIP 3	n.d.
LRIP 4	58.2 ± 19.7 nM
Scramble	n.d.

B

Compound	MBP-COR
LCIP 1	1.1 ± 0.5 μM
Scramble	n.d.[1]

C

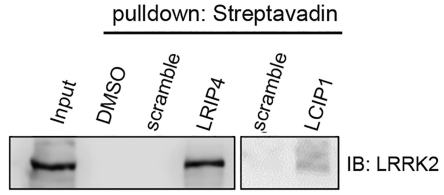

Figure 2. LCIP1 and LRIP4 bind LRRK2 *in vitro* and downregulate LRRK2 dimerization. (a) Table depicting binding affinities of each peptide in the LRIP library to MBP-RocCOR. n.d.[1] = not detected. (b) Table depicting binding affinities of LCIP1 and scramble to MBP-COR. (c) Lysates derived from HEK293 cells overexpressing GFP-tagged LRRK2 were treated with 10 μM biotin-labeled peptides (LCIP1 and LRIP4), and pulldowns were performed using avidin-coated resin. LRRK2 was detected via immunoblotting, demonstrating that both peptides pulled down LRRK2. Blot is representative of *n* = 3.

Next, we sought to determine whether the lead peptides could bind their target, LRRK2, from cell lysates. To test this, HEK293 cells overexpressing GFP-tagged LRRK2 were lysed and incubated with biotin-labeled peptides. Peptide pulldowns were performed using avidin-coated resin. As compared to DMSO and scrambled controls, LRIP4 and LCIP1 pulled down LRRK2 [Figure 2C]. Of note, LRIP4 pulled down considerably more LRRK2 as compared to LCIP1, which may correlate with this peptide binding LRRK2 with a higher affinity. To further confirm these results, pull-down experiments from cell lysates were performed and analyzed by protein mass spectrometry [Table S1]. In this experiment, LRRK2 was detected in pulldowns with either LRIP4 or LCIP1 but not their scramble controls. Both LCIP1 and LRIP4 exhibit binding to other human protein kinases including nucleoside diphosphate kinases A/B, pyruvate kinase PKM, and ribose-phosphate pyrophosphokinase 1. However, none of these kinases contain RocCOR domains and homologous proteins to LRRK2, such as LRRK1, were not found to interact with the peptides.

Peptides Permeate Cells and Inhibit Wild-Type and G2019S LRRK2 Dimerization in Cells. To determine whether LCIP1 and LRIP4 could effectively disrupt LRRK2 dimerization, we monitored disruption of dimerization using two different tagged versions of LRRK2. This was achieved by cotransfecting HEK293 cells with GFP-tagged and strep-tagged full-length LRRK2. Next, a GFP-trap immunoprecipitation (IP) was performed using lysates that were treated with or without 10 μM peptide. Western blotting was performed to detect the level of strep-tagged LRRK2. In the absence of

https://doi.org/10.1021/acschembio.1c00487
ACS Chem. Biol. 2021, 16, 2326−2338

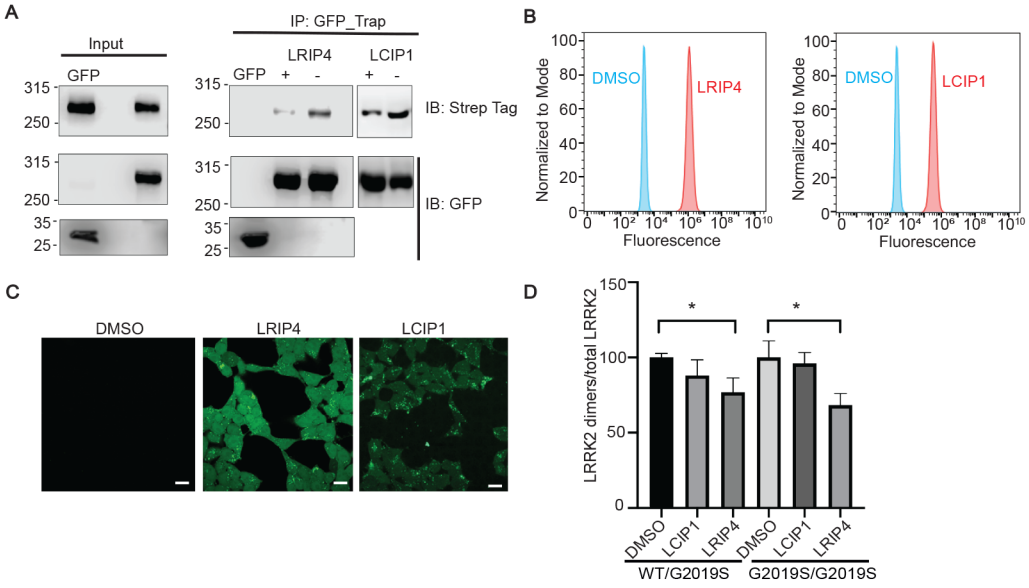

Figure 3. LCIP1 and LRIP4 permeate cells and are detected in the cytoplasm. (a) HEK293 cells were transiently transfected with strep-tagged LRRK2 and GFP or GFP-tagged LRRK2. Whereas strep-LRRK2 did not bind nonspecifically to GFP, it was pulled down with GFP-LRRK2. Incubation with inhibitory peptides LRIP4 and LCIP1 resulted in reduced dimerization. GFP alone is indicated in the bottom panel. Blot is representative of $n = 3$. (b) HEK293 cells were treated with 10 μM FAM-labeled LRIP4 or LCIP1 for 6 h at 37 °C. Flow cytometry experiments demonstrate that both peptides yielded an increased shift in fluorescence. (c) Confocal fluorescence microscopy images indicate that LRIP4 and LCIP1 can be detected in the cytosol with LRIP4 demonstrating greater cytosolic accumulation. Scale bar corresponds to 20 μm. (d) LRRK2 dimerization was measured in cells using a proximity biotinylation ELISA-based assay. Dimeric LRRK2 was biotinylated *in situ* and purified on streptavidin-coated ELISA plates. LRIP4 was found to inhibit dimerization of both wild-type/G2019S LRRK2 heterodimers and G2019S LRRK2 homodimers in HEK293 cells. *$p < 0.05$. Blot is representative of $n = 3$.

peptide treatment, strep-tagged full-length LRRK2 coprecipitated with GFP-LRRK2, indicating a background level of dimer formation [Figures 3A, S5]. Quantification of these IP experiments [Figure S5] revealed that LRIP4 and LCIP1 both downregulated LRRK2 dimerization with statistical significance as demonstrated by reduced levels of strep-tagged LRRK2. LRIP4 had the most pronounced effect with approximately 70% reduction, albeit neither peptide yielded complete inhibition of dimer formation.

To establish whether LCIP1 and LRIP4 would be suitable for cell-based experiments, cell permeation of the peptides was evaluated. Flow cytometry revealed dose-dependent uptake of both lead peptides [Figure S6]. At the 6-h time point, both peptides demonstrated considerable permeability as measured by a shift in fluorescence detection by flow cytometry [Figures 3B, S6]. To determine whether the peptides could reach the cytosol, confocal microscopy was performed. While both peptides were detected in the cytoplasm, LRIP4 had greater cytoplasmic fluorescence intensity as well as some nuclear localization, while LCIP1 appeared to partly localize within vesicles [Figure 3C].

We next sought to assess whether these peptides could also inhibit LRRK2 dimer formation in cells. We used a previously published *in situ* LRRK2 proximity biotinylation approach[46] where HEK293T cells expressing either wild-type or G2019S mutants of LRRK2 fusions, either with the biotin ligase BirA or the acceptor peptide AP, were treated with increasing concentrations (0.1, 1, and 10 μM) of each fluorescently labeled peptide. The ROC domain-targeting peptide, LRIP4, caused a statistically significant reduction in both G2019S/G2019S and G2019S/wild-type LRRK2 dimers at 10 μM peptide treatment [Figures 3D, S7–S9. In this assay, LCIP1 failed to consistently lead to a reduction in LRRK2 dimerization [Figures S7, S8] which may be due to relatively weaker cell permeation and weaker target binding as compared to LRIP4. Further, only partial inhibition could be observed, and this may be due to many other interfaces involved in LRRK2 dimerization derived from other domains of the protein that may still influence and induce dimerization.

Disrupting LRRK2 Dimerization Attenuates LRRK2 Kinase Activity but Does Not Induce Mislocalization. Autophosphorylation at site S1292 is correlated with LRRK2 kinase activity.[47] To test whether impaired LRRK2 dimerization may result in LRRK2 kinase activity, we therefore measured the effects of LRIP4 and LCIP1 on LRRK2 S1292 phosphorylation. In these experiments, HEK293 cells were transfected with GFP-tagged LRRK2. Cells were then treated with 10 μM of either LRIP4 or LCIP1 prior to immunoblotting. Western blots of pS1292-LRRK2 revealed that both peptides caused a significant reduction of autophosphorylation by 50–70% as compared to the DMSO control, although neither was as potent as the ATP-competitive LRRK2 inhibitor MLi-2 [Figure 4A,B].

LRRK2 kinase activity was also measured as a function of Rab10 phosphorylation.[48,49] To test whether disruption of LRRK2 dimerization can also reduce Rab phosphorylation, a hyperactive LRRK2 mutant (R1441G) and Rab29 were overexpressed in HEK293T cells.[50,51] Overexpression of Rab29 induces recruitment of LRRK2 to the trans-golgi network (TGN) where it becomes activated. After transfection, cells were then treated with 10 μM peptide, followed by immunoblotting of pT73 Rab10. In these experiments, treatment with LRIP4 or LCIP1 reduced Rab10 phosphorylation with LRIP4 inducing a more pronounced effect [Figure 4C]. We performed a homologous experiment in cells transfected with LRRK2 G2019S and show that LRIP4

https://doi.org/10.1021/acschembio.1c00487
ACS Chem. Biol. 2021, 16, 2326–2338

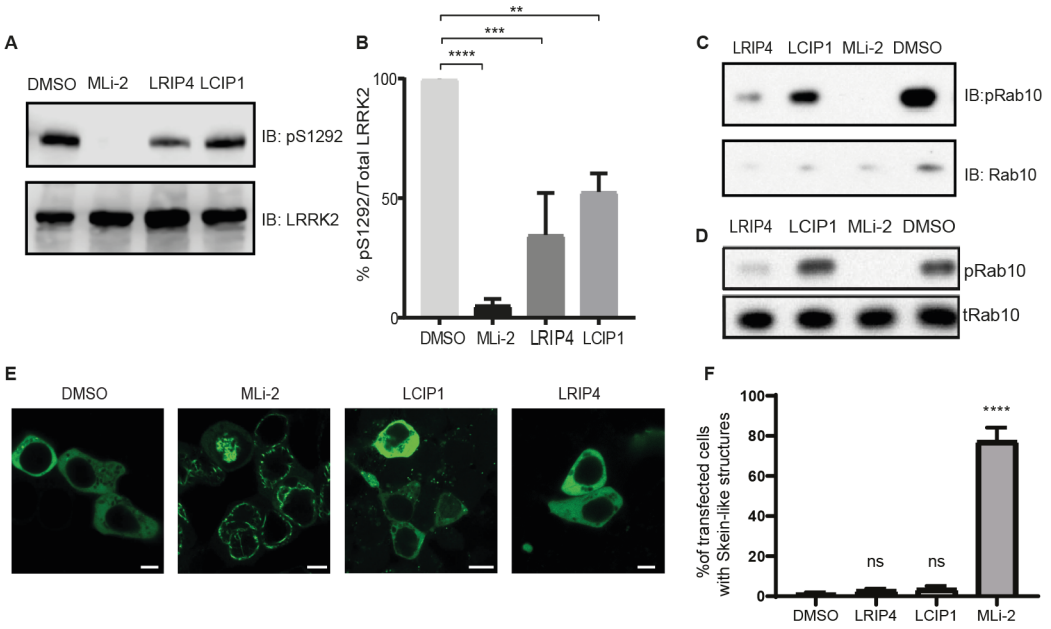

Figure 4. LRIP4 inhibits LRRK2 autophosphorylation and Rab10 phosphorylation. (a) Autophosphorylation of LRRK2 (pS1292) was monitored in HEK293 cells in the presence of inhibitor peptides (10 μM) or the ATP-competitive LRRK2 inhibitor MLi-2 (100 nM). Both peptides inhibited LRRK2 autophosphorylation as compared to the DMSO control. Blot is representative of $n = 3$. (b) Quantification of a by-densitometric analysis. Levels of pS1292-LRRK2 were normalized to total LRRK2 expression and shown as LRRK2 activity relative to the DMSO control. Data were averaged from three independent experiments and are shown as means ± SD. The inhibitor peptides downregulated autophosphorylation by 50−70% but not as potently as MLi-2. (c) HEK293T cells were transfected with SF-tagged LRRK2 (R1441G) and FLAG-HA-tagged Rab29 and treated with 10 μM of inhibitor peptides for 12 h prior to lysis. Endogenous Rab10 phosphorylation was reduced after treatment with LRIP4 or LCIP1, with LRIP4 having a larger inhibitory effect. (d) Untransfected A549 cells were used to investigate the inhibitory effect of LRIP4 and LCIP1 (10 μM) on endogenous LRRK2 kinase activity as measured by Rab10 phosphorylation. LRIP4 downregulated Rab10 phosphorylation. (e) HEK293 cells were transiently transfected with GFP-tagged LRRK2 and treated with biotin-labeled peptides (10 μM of LRIP4 or LCIP1) for 12 h. As a control, cells were treated with 100 nM MLi-2. Unlike cells treated with MLi-2, LRIP4 and LCIP1 did not induce mislocalization of LRRK2 in cells. Scale bar represents 5 μm. Images are representative of $n = 3$. (f) Quantification of the results in e is shown. A minimum of 200 transfected cells were analyzed under each condition for filamentous structures of GFP-LRRK2. The average percentage of cells showing skein-like structures and standard errors of the mean (SEM) for three biological replicates are shown. ****$p < 0.0001$.

reduced Rab10 phosphorylation and LRRK2 autophosphorylation at pS1292; however, LCIP1 had no effect [Figure S10]. To test the effect of the dimerization inhibitors on endogenous LRRK2 function, we performed a similar experiment using nontransfected A549 cells which natively express detectable levels of both LRRK2 and Rab10. In these cells, LRIP4 caused a significant reduction in phosphorylation of Rab10 as compared to the DMSO control [Figures 4D, S11]. On the other hand, LCIP1 had a modest effect on Rab10 phosphorylation. This may be due to variances in different cell lines for the different experiments, the extent of permeation by the compound, or differences in LRRK2 localization and expression levels. To measure whether disruption of dimerization would alter the GTPase activity of LRRK2, full-length wild type LRRK2 was incubated with 10 μM of peptide and GDP production was measured via reversed phase HPLC. The peptides did not induce a change in the intrinsic hydrolysis of the monomer, indicating no effect on GTPase activity [Figure S12]. Together, it appears that disrupted dimerization may lead to reduced LRRK2 activation as assessed by autophosphorylation of LRRK2 and subsequent Rab10 phosphorylation. This demonstrates that LRRK2 dimerization may control LRRK2 kinase activation and disruption of dimerization may allosterically inhibit LRRK2 activity.

Next, we analyzed the effects of these inhibitor peptides on LRRK2 localization. Classical ATP-competitive LRRK2 kinase inhibitors induce cellular recruitment of LRRK2 to microtubules and block kinesin and dynein-1-mediated transport.[28,52] To investigate whether the dimerization-blocking peptides would induce a similar phenotype, the localization of GFP-tagged LRRK2 was analyzed by confocal microscopy [Figures 4E,F]. Consistent with previous studies, the LRRK2 ATP-competitive inhibitor MLi-2 induced altered localization to filament-like structures. This is also consistent with previous work demonstrating that kinase inhibitor-induced filaments are populated with dimeric LRRK2.[21] In contrast, LRRK2 maintained its cytoplasmic distribution after 12-h treatments with 10 μM of either LRIP4 or LCIP1. On the basis of this observation, it is possible that allosterically inhibited monomeric LRRK2 may be adopting a different conformation as compared to catalytically inhibited LRRK2.

Targeting LRRK2 Dimerization Inhibits LRRK2-Mediated ROS Production and Neuronal Apoptosis. We subsequently sought to evaluate how these peptide inhibitors of LRRK2 impact PD-linked cellular effects. Although the exact physiological function of LRRK2 is still elusive, and in particular the mechanism(s) by which mutant forms induce neuronal death, pathogenic LRRK2 mutants were shown to impair lysosomal function and therefore account for increased levels of ROS production[53] in both neuronal[54,55] and peripheral immune cells.[56,57] Further, inhibition of LRRK2 kinase activity was reported to alleviate such enhanced oxidative stress.[54,56,57] Consistent with these observations,

https://doi.org/10.1021/acschembio.1c00487
ACS Chem. Biol. 2021, 16, 2326−2338

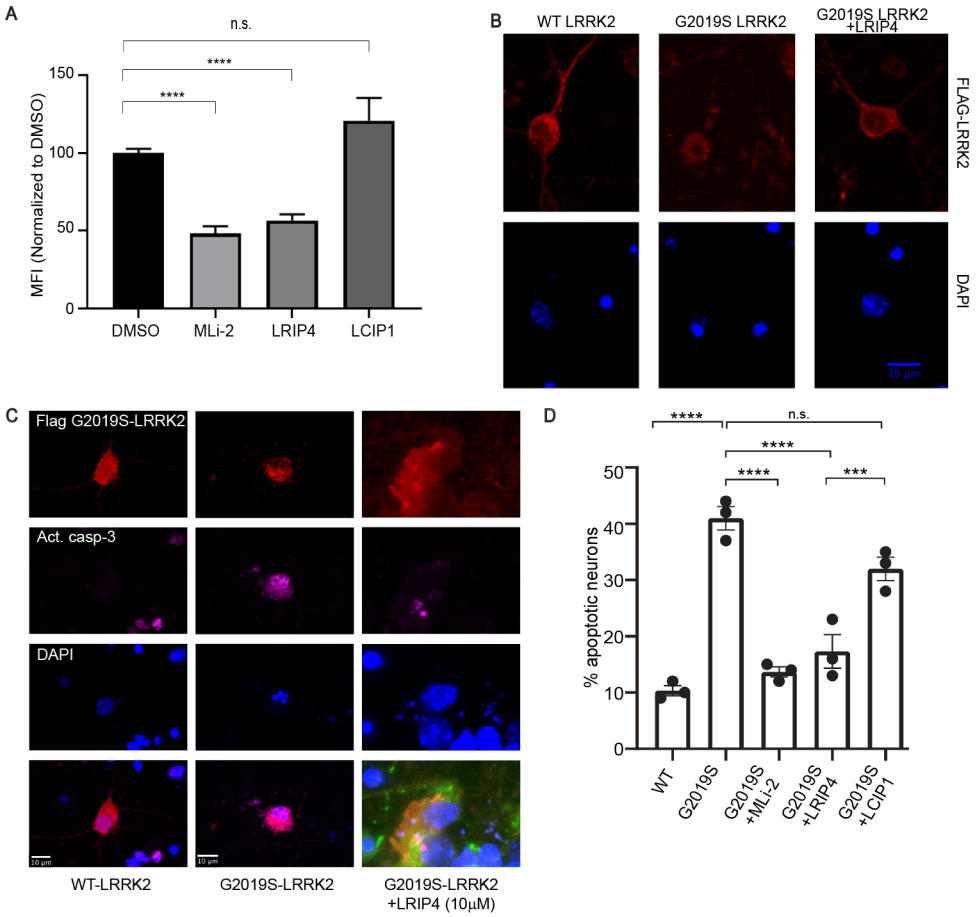

Figure 5. LRIP4 downregulates ROS production and neuronal apoptosis. (a) Reactive oxygen species (ROS) were measured via fluorescence emission of the CellROX deep red dye. RAW 264.7 cells were treated with 10 μM of each peptide for 9 h and then stimulated with Zymosan for 30 min (50 μg/mL). LRIP4 significantly downregulated ROS production, $n = 4$. (b) Cultured primary cortical neurons transiently overexpressing WT or G2019S-LRRK2 were treated with 10 μM of each peptide for 48 h, or 200 nM of MLi-2. Fixed neurons were immunostained for flag-LRRK2 and counterstained with DAPI. Scale bar represents 10 μm, $n = 3$. (c) Primary neurons were transiently transfected with Flag-LRRK2 (WT, G2019S) and then treated the following day with 10 μM LRIP4 for a total of 48 h (72 h total transgene overexpression). Neurons were fixed and immunostained for Flag and an active form of caspase-3, which strictly colocalizes in neurons with condensed/fragmented (two or more) nuclei. (d) Quantification of apoptotic neurons from c. Neurons from three biological replicates (independent transfections) were counted in a blinded manner, $n = 3$. *$p < 0.05$; **$p < 0.01$; ***$p < 0.001$; ****$p < 0.0001$.

incubation of cells with LRIP4 resulted in a significant reduction of zymosan induced ROS production to an extent comparable to MLi-2 [Figure 5A]. The effect of LCIP1 on ROS production produced highly variable results, similar to its effects on dimerization in cells, thereby yielding no statistically significant consequence.

Finally, we used primary cortical neurons to assess the neuroprotective ability of LRIP4 and LCIP1. It has been shown that LRRK2-mediated neuronal toxicity is kinase-dependent.[58] To determine if peptide-treated cortical neurons maintained cellular integrity, fluorescence imaging was performed.[59] Cortical neurons transfected with wild-type LRRK2 maintained proper cellular morphology, with no evidence of nuclear changes typical of apoptotic death, whereas neurons expressing G2019S LRRK2 exhibited aberrant LRRK2 distribution and apoptotic nuclear condensation and fragmentation and activation of the late-stage protease caspase-3 [Figure 5B,C]. Importantly, upon treatment with the peptides, there was a sharp decline in neurons undergoing apoptosis, especially for LRIP4 treated cells [Figure 5D]. Furthermore, we sought to determine whether pharmacodynamic markers of kinase inhibition are evident in primary neurons treated with the peptides, expressing endogenous levels of LRRK2. After overnight treatment with LRIP4 or LCIP1, we saw a statistically significant decrease in pS935 relative to the scramble treated control, similar to what is seen following treatment with MLi2 [Figure S13]. Together, these results indicate that disruption of dimerization with LRIP4 can effectively downregulate LRRK2-mediated ROS production, kinase activity, and neuronal apoptosis.

DISCUSSION

Although the normal function of LRRK2 is not fully understood, elevated kinase activity in both PD-linked mutations and idiopathic PD leads to neuronal degeneration.[3−11] Further, inhibition of abnormally elevated activity of PD-associated LRRK2 can result in neuroprotection.[12] Although LRRK2 has been sought after as a therapeutic target for PD, the ATP-competitive LRRK2 kinase inhibitors reported to date have largely led to altered LRRK2 localization as well as kidney and lung abnormalities in *in vivo* toxicological studies.[19,60,61] Thus, alternative strategies to downregulate

https://doi.org/10.1021/acschembio.1c00487
ACS Chem. Biol. 2021, 16, 2326−2338

LRRK2 activity could present new opportunities for targeted therapeutic intervention.

LRRK2 was previously shown to alternate between monomeric and dimeric species where LRRK2 exists primarily as a dimer with enhanced kinase activity is associated with the dimeric fractions of LRRK2.[46,62] Further, LRRK2 dimers were also shown to exist inside cells and are enriched at membranous structures with proportionally little dimeric LRRK2 in the cytosol.[51,63] In addition, LRRK2 kinase activity was found to be induced upon dimerization,[64] which is at least partly mediated by intermolecular interactions between the RocCOR tandem domains of two LRRK2 monomers. The mechanism regulating the balance between the monomer/dimer population is not known,[44,64−66] although it is clear that GDP/GTP binding to the RocCOR domain plays a role in regulating this equilibrium.[41,67] While most pathogenic variants of LRRK2 are associated with either increased kinase or decreased GTPase activity, it was also recently shown that wild-type LRRK2 kinase activity was enhanced in midbrain DA neurons of patients with idiopathic PD.[17] Therefore, allosteric targeting of LRRK2 to regulate dimerization may serve as a strategy to shift from the dimer to monomer population and may be a viable alternative strategy for targeted inhibition of kinase activity, without altering its localization. We previously showed that disruption of dimerization using nanobodies can increase the GTPase activity in a bacterial homologue of LRRK2.[67]

Here, we report the design, synthesis, and characterization of a peptide-based PPI inhibitor of LRRK2 dimerization, namely LRIP4. LRIP4 was shown to permeate cells, inhibit dimerization, and inhibit kinase activity both *in vitro* and in cells. Although the exact physiological function of LRRK2 is still elusive, and in particular the mechanism(s) by which mutant forms induce neuronal death, pathogenic LRRK2 mutants were shown to impair lysosomal function and therefore account for increased levels of ROS production[53] in both neuronal[54,55] and peripheral immune cells.[57] Consistently, inhibition of dimerization also led to reduced ROS production and neuronal apoptosis. In addition, we demonstrate for the first time that this inhibition strategy can downregulate kinase activity without inducing LRRK2 mislocalization that was previously shown by ATP-competitive kinase inhibitors of LRRK2. To our knowledge, this study is the first report of allosteric inhibition of LRRK2 dimerization and provides pharmacological evidence that LRRK2 dimerization regulates kinase activity. Our second compound, LCIP1, which targeted the COR domain, showed limited cell uptake and binding affinity when compared to LRIP4. Although this compound showed some inhibitory activity in early biochemical assays, it had little to no activity in cells. Previous reports indicate that the COR domain is essential for mediating dimerization;[22,40] therefore, optimization of this targeting site based on recent structural advances could result in a more potent disruptor of dimerization. Several limitations exist for studying allosteric inhibitors of LRRK2 including low LRRK2 expression levels in many cell lines and the need to transfect some cell lines to promote detectable levels of phospho-Rab10. Further, biochemical experiments with LRRK2 remain difficult due to challenges with stable expression and purification of full-length or truncated constructs of LRRK2 as well as the tendency of LRRK2 protein to dimerize in solution.

To further explore the potential for targeting LRRK2 dimerization, high-resolution structural insights into LRRK2 are required. Even though the exact function of the RocCOR domain is unknown, our results demonstrate that disruption of RocCOR-mediated dimerization attenuates LRRK2 kinase activity. Recently published structures reveal many new interfaces that are critical for LRRK2 dimerization and may also serve as viable targets for LRRK2 inhibition.[27−29] In addition, allosteric disruptors will be invaluable tools to dissect the different functions of the many domains of LRRK2 as we seek to better understand the significance of each domain on LRRK2 activity and regulation.

METHODS

Constructs. Cloning of the Strep-FLAG (SF) tagged LRRK2 (pDEST(N)SF.LRRK2 constructs has been described previously.[44] The generation of N-terminal Flag-tagged LRRK2 for the transfection of neuronal cultures has been described in ref 66. N-terminal GFP-tagged LRRK2 (pcDNA3.1_GFP.LRRK2) has been generated by Gateway cloning. For the proximity biotinylation assay, two constructs were created encoding LRRK2 fusions with biotin ligase (BirA; N-term, Flag-tagged) and an acceptor peptide (AP, N-term; c-Myc tagged).[46] The cDNAs encoding Rab10 and Rab29 were ordered as synthetic genes and subcloned via the Gateway system into the pcDNA3.0-based pDEST N-HA/FLAG vector, generated in-house.

Cell Culture. LRRK2 parental RAW 264.7 cells (ATCC, SC-6003) were cultured in Dulbecco's Modified Eagle's medium (DMEM, ATCC, 30-2002) supplemented with 10% FBS and 1% penicillin-streptomycin (Gibco, 15070063). HEK293(T) cells (ATCC, CRL-1573, and CRL-3216) and A549 cells (ATCC, CCL-185) were grown in Dulbecco's Modified Eagle's medium (DMEM, Gibco, 11960044) supplemented with 10% FBS and 1% penicillin-streptomycin-Glutamine (Gibco, 10378016).

Peptide Synthesis. Peptide synthesis was performed using standard Fmoc solid phase peptide synthesis on Rink amide MBHA resin using standard N-α-Fmoc amino acids. All synthesis reagents and solvents were purchased from Fisher, Sigma-Aldrich, or Acros. Deprotection was performed using 25% (v/v) piperidine in 75% (v/v) *N*-methylpyrrolidinone (NMP) for 25 min with agitation. After each deprotection, resin was washed three times for 30 s with NMP and agitation. Standard amino acids were coupled by adding 10 equiv of amino acids followed by the addition of 9.9 equiv of 2-(6-chloro-1H-benzotriazole-1-yl)-1,1,3,3-tetramethylaminium hexafluorophosphate (HCTU in NMP). Twenty equivalents of N,N-diisopropyl ethylamine (DIEA, Fisher) was added to catalyze the addition of the amino acid. This solution was agitated for 45 min. For S_5 ((S)-N-Fmoc-2-(4-pentenyl) alanine, Sigma-Aldrich) and PEG_3 (Fmoc-11-amino-3,6,9-trioxaundecanoic acid, ChemPep), we added 4 equiv of S_5 or PEG_3, followed by the addition of 3.9 equiv of HCTU. For LRIP4, Methionine 1466 was mutated to norleucine to improve synthetic yield. This substitution was contingent on evidence suggesting the methionine was not essential for mediating dimerization.

To cyclize the olefinic amino acids and form the staple, we performed ring closing metathesis (RCM) using a first generation Grubbs catalyst. This reaction was performed on resin with 1,2-dichloroethane (DCE) using 0.4 equiv of a first generation Grubbs catalyst for two separate 1-h time periods. Upon completion of the sequence and closing of the staple, we made modifications to the N-terminus based on experimental needs. These modifications included the addition of a PEG_3 linker (previously described[36]) and labeling with either 5,6-carboxyfluorescein (FAM, Sigma-Aldrich) or D-biotin (GoldBio). For FAM labeling, 2 equiv of FAM were added with 1.8 equiv of HCTU and 4.6 equiv of DIEA overnight in dimethylformamide (DMF) with agitation. For biotin labeling, 10 equiv of biotin were added with 9.9 equiv of HCTU and 20 equiv of DIEA in a 1:1 mixture of dimethyl sulfoxide (DMSO) and DMF overnight with agitation. After overnight labeling, the peptides were cleaved from resin using 95% (v/v) trifluoroacetic acid (TFA), 2.5% (v/v)

https://doi.org/10.1021/acschembio.1c00487
ACS Chem. Biol. 2021, 16, 2326−2338

triisopropylsilane, and 2.5% (v/v) water then rotated for 5 h at RT. Peptides were then precipitated in methyl-*tert*-butyl ether at 4 °C via centrifugation.

Peptide Characterization. Following cleavage from resin, peptides were separated via RP-HPLC using a Zorbax analytical SB-C18 column. The mobile phase linear gradient was 10−100% water to acetonitrile with 0.1% TFA at a flow rate of 0.5 mL/min. Peptides were then characterized via ESI-MS (Agilent 6120 Single Quadrupole) following separation over a Zorbax analytical SB-C18 column via HPLC (Agilent 1200). Peptide purification was performed using the same conditions over a semipreparatory column with a flow rate of 4 mL/min. To confirm peptide purity, products were analyzed by ESI-MS over a Zorbax analytical SB-C18 column.

To quantify peptides, intrinsic qualities of the N-terminal labels were used. For FAM labeled peptides, quantification was based on the absorbance at 495 nm in 10 mM Tris (pH 8) using an extinction coefficient of 69 000 $M^{-1}cm^{-1}$. Biotin-labeled peptides were quantified by measuring decreased absorbance of the 2-hydroxyazobenzen-4′-carboxylic acid (HABA)-avidin complex at 500 nm. Final M/S for all peptides are included in the Supporting Information (norleucine is abbreviated Nle; Figures S14−S21).

The peptide sequence for FAM-labeled LRIP1 is 5(6)FAM-PEG_3-DEK*RKA*(Nle)SKITKELLNKR, and the mass is 2967.0 (expected = 2967.5).

The peptide sequence for FAM-labeled LRIP2 is 5(6)FAM-PEG_3-DEKQRKA*(Nle)SK*TKELLNKR, and the mass is 2981.4 (expected = 2982.4).

The peptide sequence for FAM-labeled LRIP3 is 5(6)FAM-PEG_3-DEKQRKAC(Nle)SK*TKE*LNKR, and the mass is 2972.0 (expected = 2972.4).

The peptide sequence for FAM-labeled LRIP4 is 5(6)FAM-PEG_3-DEKQRKAC(Nle)SKITKE*LNK*, and the mass is 2928.0 (expected = 2929.4).

The peptide sequence for Biotin-labeled LRIP4 is D-Biotin-PEG3-DEKQRKAC(Nle)SKITKE(S5)LNK(S5), and the mass is 2796.6 (expected = 2797.4).

The peptide sequence for FAM-labeled LRIP4 scramble is 5(6)FAM-PEG_3-Q(Nle)DKAESKNKERKLC*TIK*, and the mass is 2928.9 (expected = 2929.4).

The peptide sequence for Biotin-labeled LRIP4 scramble is D-Biotin-PEG_3-Q(Nle)DKAESKNKERKLC*TIK*, and the mass is 2796.9 (expected = 2797.4).

The peptide sequence for FAM-labeled LCIP1 is 5(6)FAM-PEG_3-KGEGE*LLK*WK, and the mass is 1983.6 (expected = 1984.3).

The peptide sequence for Biotin-labeled LCIP1 is D-Biotin-PEG_3-KGEGE*LLK*WK, and the mass is 1851.6 (expected = 1852.3).

The peptide sequence for FAM-labeled LCIP1 scramble is 5(6)FAM-PEG_3-GKWEK*GEL*KL, and the mass is 1983.6 (expected = 1984.3).

The peptide sequence for Biotin-labeled LCIP1 scramble is D-Biotin-PEG_3- GKWEK*GEL*KL, and the mass is 1851.6 (expected mass = 1852.3).

The peptide sequence for FAM-labeled LRIP Native is 5(6)FAM-PEG3-DEKQRKAC(Nle)SKITKELLNKR, and the mass is 2946.9 (expected = 2948.4).

Fluorescence Polarization (FP) Assays. Direct binding of our lead compounds (LRIP4 and LCIP1) to LRRK2 constructs was assessed via FP assays. For LRIP4, we measured binding with purified MBP-tagged RocCOR LRRK2 protein in the presence of 2 mM GTP and 10 mM $MgCl_2$. For LCIP1, we measured binding to purified MBP-tagged CORB. Each FAM-labeled peptide was plated at a final in-well concentration of 10 nM in 384-well microtiter plates. 1:2 dilutions of the protein were then performed from a concentration range of 5 μM to 1 nM. For each peptide/protein interaction, we had a range of at least 10 protein concentrations, and each concentration was performed in triplicate. The assay was performed in FP buffer (20 mM MOPS pH 7, 150 mM NaCl, and 0.005% CHAPS) at RT. The peptide/protein mixture was incubated at RT for 2 h with readings taken every 30 min. The final readings were obtained at 2 h.

Protein Mass Spectrometry Analysis of Binding Interactors in Cells. Proteins interacting with biotin-labeled LRIP4, LRIP4 Scramble, LCIP1, or LCIP1 Scramble peptides were captured by magnetic strep-beads as described in pulldown experiments. The samples were denatured with 1.6 M urea, reduced with 5 mM TCEP (37 °C, 1h), alkylated with 10 mM iodoacetamide (RT, 45 min in dark), and digested with sequencing grade modified trypsin (37 °C, overnight). After digestion, the magnetic beads were removed from the samples, and the tryptic peptides were extracted by solid phase extraction using C18 tips (Pierce). The cleaned peptides were then subjected to LC-MS analysis using an Easy-nLC II LC system coupled to a LTQ Orbitrap XL mass analyzer (Thermo Scientific). The data acquisition was set at data-dependent mode for 60 min elution gradient, with full scan MS spectra (m/z 300−1650) at a resolution of 30 000. The raw data were imported into PEAKS Studio X+ (Bioinformatics Solutions Inc.) and analyzed against all reviewed human proteins in the Uniprot database. The peptide false discovery rate (FDR) was set to 0.1% using the target-decoy method. Protein entries with at least one unique peptide found in the analysis were regarded as positive hits and tabulated.

Pulldown Experiments. Fresh lysate of HEK293 cells overexpressing GFP-tagged LRRK2 was mixed and incubated with biotin-labeled peptide (added to a final concentration of 10 μM) and incubated at 4 °C overnight. The mixture was then applied to Magnetic Strep-beads (MagStrep "Type3" XT Beads (IBA, Göttingen, Germany)), and the immune complex was washed twice (10 mM Tris/HCl pH 7.5, 150 mM NaCl) and subjected to immunoblot analysis. Samples were separated on 6% Tris-Glycine gels, transferred onto a nitrocellulose membrane (GE Lifesciences), and processed for western analysis. Membranes were blocked in 5% dry milk in Tris-buffered saline plus Tween-20 for 1 h and probed with rat monoclonal anti-LRRK2 (clone 24D8 1:1000, Gloeckner lab[68]) and incubated overnight at 4 °C with gentle shaking. Membranes were then washed three times for 10 min at RT in PBS containing 0.1% or 0.05% Tween-20 and then incubated for 1 h with antirat IgG-HRP (sc-2750, Santa Cruz Biotechnology). Membranes were again washed three times for 10 min at RT in PBS containing 0.1% or 0.05 Tween-20. The membranes were coated with an enhanced chemiluminescent (ECL) reagent (WesternSure PREMIUM, Li-COR biosciences), and proteins were detected using the C−Digit Imaging System (Li-COR Biosciences).

In Vitro Dimerization Assay. HEK293 cells were cotransfected using JetPEI reagent (Polyplus transfection) with pcDNA3.1_GFP.LRRK2 and pDEST(N)SF.LRRK2. Cells were cultivated for 48 h. The cells were then lysed with 200 μL of ice-cold lysis buffer (10 mM Tris/HCl pH 7.5; 150 mM NaCl; 0.5 mM EDTA; 0.5% NP-40), complete EDTA-free protease inhibitor cocktail (Sigma−Aldrich Cat # 11836170001), and Protease Inhibitor Cocktail, Sigma (cat. no. P-2714). The mixture was incubated and rotated on ice for 30 min with extensive pipetting every 10 min. Lysate was cleared by centrifugation for 10 min at 14 000g for 10 min at 4 °C. The supernatant was transferred to a precooled tube, and 300 μL of dilution buffer (same as lysis buffer without NP-40) was added to the lysate. Peptides were added to a final concentration of 10 μM, and the mixture was allowed to rotate at 4 °C overnight. GFP-LRRK2 was immunoprecipitated with Magnetic GFP nanotrap beads (ChromoTek). Immune complexes were washed twice with 10 mM Tris/HCl at pH 7.5 and subjected to immunoblot analysis by boiling samples in sample buffer with a reducing agent. Samples were separated on 6% Tris-Glycine gels, transferred onto a nitrocellulose membrane (GE Healthcare), and processed for western analysis. Membranes were blocked in 5% dry milk in Tris-buffered saline plus Tween-20 for 1 h and probed with mouse anti-Strep tag LRRK2, 1:1000 (34850, Qiagen), or rabbit anti-GFP antibodies, 1:2500 (MA5−15256, Invitrogen), and incubated overnight at 4 °C with gentle shaking. Membranes were then washed three times for 10 min at RT in PBS containing 0.1% or 0.05% Tween 20 and then incubated for at least 1 h (light protected) with secondary antibodies: mouse IgG kappa binding protein (m-IgGκ BP) conjugated to horseradish peroxidase (HRP; sc-516102, Santa Cruz Biotechnology, 1:5000) or

https://doi.org/10.1021/acschembio.1c00487
ACS Chem. Biol. 2021, 16, 2326−2338

antirabbit HRP conjugated (#7074, Cell Signaling, 1:500). Membranes were again washed three times for 10 min at RT in PBS containing 0.1% or 0.05% Tween-20. The membranes were coated with the enhanced chemiluminescent (ECL) reagent (WesternSure PREMIUM, Li-COR biosciences), and proteins were detected using the C−Digit Imaging System (Li-COR Biosciences).

Flow Cytometry. HEK293 cells were plated in 96-well plates (50 000/well) and allowed to grow 24 h in complete growth medium (DMEM supplemented with 10% fetal bovine serum, L-glutamine). DMEM was carefully aspirated, and cells were treated with fresh prewarmed complete growth medium supplemented with 10 μM of peptide or DMSO. After 6 h, cells were analyzed on a Beckman Cytoflex flow cytometer (Beckman Coulter). Using forward and side scattered light, a gate for intact, nonaggregated cells was defined, and the fluorescence of 10 000 events was collected within this cell gate. The fluorescent channel for FITC (488 nm excitation [ex], 525 nm emission [em]) was used. Data were analyzed using FlowJo software, and the reported fluorescent intensity values represent arithmetic means of the results determined for the analyzed cells.

Confocal Microscopy. HEK293 cells were plated (40 000/well) on μ-Slides (chambered coverslip, tissue-culture treated, 80826, Ibidi) and cultured for 24 h in complete growth medium (DMEM supplemented with 10% fetal bovine serum and L-glutamine). Then, DMEM was carefully aspirated, and cells were treated with fresh prewarmed growth medium (DMEM supplemented with FAM-labeled stapled peptide (10 μM) or DMSO). After 6 h, cells were washed three times in warm PBS to remove excess peptide from the cell surface and left in prewarmed low fluorescence imaging medium (FluoroBrite DMEM, Gibco). Cells were immediately analyzed under an LSM800 confocal laser scanning microscope with a prewarmed incubation chamber (37 °C). By scanning through the z planes of each cell, the outer plasma membrane borders were determined. Images were taken between the plasma membrane z planes to obtain signals from internalized peptides and to minimize artificial signals from cell surface adhered peptides. The distribution of FAM-labeled peptides was analyzed using a 63X Plan-Apochromat oil-immersion objective (Zeiss). Image analysis of z-scan was done using the Zeiss microscope software ZEN.

Proximity Biotinylation of Dimeric LRRK2. To purify LRRK2 dimers, we relied on the proximity biotinylation technique recently described.[46,69] Briefly, two cDNAs were created encoding LRRK2 fusions with biotin ligase (BirA; N-term, Flag-tagged) and an acceptor peptide (AP, N-term; c-Myc tagged) and overexpressed in HEK293T cells grown in biotin-depleted medium (OptiMEM+2% FBS). The following day, the cells were treated with the indicated concentrations of the stapled peptides: LRIP4 and LCIP1. Stock peptides, fluorescently tagged, were diluted in serum-free medium and added every 24 h after transfection. After 48 h, following the initiation of treatment (i.e., 72 h of total expression), the cells were extensively washed in PBS, given a brief biotin pulse (50 μM, 5 min, 37°C), followed by another three washes in PBS, and centrifuged and the pellet snap frozen in a dry ice/MeOH bath. In some experiments, the cells were treated with peptides for a total of 24 h before collection. Following lysis, extracts were diluted in TBST/BSA (10 mM Tris HCl, pH 7.6; 100 mM NaCl; 0.1% Triton X-100; 1% BSA) and 2.5 μg of protein loaded in parallel ELISA plates, coated with streptavidin (SA; to capture biotinylated LRRK2 dimers) and anti-LRRK2 (to quantify LRRK2 overexpression). To detect and quantify dimeric LRRK2, SA-coated plates were incubated with HRP-conjugated anti-Flag antibodies (1 h, RT). Since the biotin tag is only present on AP-LRRK2 fusions, and the flag epitope tag is located on the BirA-LRRK2 fusion, by using HRP-Flag as our detector reagent, we are specifically labeling dimeric LRRK2 present in the ELISA plates. On the parallel anti-LRRK2 coated plates (clone c41−2), total overexpressed LRRK2 was quantified using HRP-LRRK2 antibodies (clone N241) and used to normalize the relative amounts of dimeric LRRK2. We assessed the following LRRK2 dimers: WT/WT homodimers, WT/G2019S, and G2019S/G2019S homodimers.

LRRK2 Immunoblotting. Protein content per sample was determined by a bicinchoninic acid colorimetric assay (BCA), using bovine serum albumin as a standard (23225; Life Technologies). Next, 100 μg of protein was resolved on 6% Tris-glycine gels and transferred to a nitrocellulose membrane (GE Lifesciences). Membranes were then blocked in 5% dry milk in Tris-buffered saline plus Tween-20 for 1 h and probed with rabbit anti-LRRK2-pSer1292 (1:1000, ab203181, Abcam) overnight at 4 °C. Membranes were washed three times for 10 min at RT in PBS containing 0.1% or 0.05% Tween 20 and then incubated for 1 h with antirabbit HRP conjugated (1:500, #7074, Cell Signaling). The membranes were coated with the enhanced chemiluminescent (ECL) reagent (WesternSure PREMIUM, Li-COR biosciences), and proteins were detected by C−Digit Imaging System (Li-COR Biosciences). For total LRRK2 detection, membranes were subsequently stripped (0.2 M Glycine pH 2.2, 0.1% SDS, 1% Tween-20), reblocked as above, and probed with rat monoclonal anti-LRRK2 (clone 24D8, 1:1000, Gloeckner lab[68]) overnight at 4 °C. Membranes were then incubated with antirat IgG-HRP (sc-2750, Santa Cruz Biotechnology). Membranes were again washed three times for 10 min at RT in PBS containing 0.1% or 0.05 Tween 20. The membranes were coated with enhanced chemiluminescent (ECL) reagent (WesternSure PREMIUM, Li-COR biosciences), and proteins were detected with a C−Digit Imaging System (Li-COR Biosciences). For quantification, images were analyzed with Image Studio (Li-COR), and signals were normalized to total LRRK2 and expressed as percentage of within-gel DMSO controls.

Rab10 Immunoblotting. HEK293T cells were cotransfected at a confluency of 50−60% with Strep-FLAG tagged LRRK2 R1441G and Rab29 as well as Rab10 (both HA-FLAG tagged) using polyethylenimine (PEI, Polyscience) as previously described.[44] At a confluency of approximately 80%, cells were treated with either 1 μM MLi-2, DMSO, or 10 μM of LRIP4 or LCIP1. After an additional 15 h, cells were lysed twice, first in lysis buffer (30 mM Tris-HCL (pH7.4), 150 mM NaCl, 0.5% NP-40, complete protease Inhibitor cocktail, and phosphatase inhibitor cocktail II and III (Sigma-Aldrich), and again after centrifugation in 1% SDS. Cleared lysates were adjusted to 2 μg/μL with 5 × Laemmli Buffer and lysis buffer. Samples were used for denaturating electrophoresis using 10% Bis-Tris gels (NuPAGE) and for Western blotting onto PVDF membranes. Membranes were blocked with 5% nonfat dry milk dissolved in TBS-T (30 mM Tris-HCL (pH 7.4), 0.1% Tween 20) and separated horizontally at 140 kDa. Primary antibodies were added TBS-T with 5% BSA (pT73 Rab10) 1:2000 (ab230261) and pS1292 LRRK2 1:2000 (ab203181)) or total protein antibodies (Rab10-(ERP13424) 1:5000 (ab181367) or LRRK2(clone 24D8) 1:5000 (Gloeckner lab)), respectively. Membranes were incubated with HRP-conjugated secondary antibodies diluted in TBS-T with 5% milk prior to imaging using ECL Plus (Pierce) with exposure to photometric films (Hyperfilms, GE Healthcare).

In Vitro GTPase Assay. Different concentrations of full-length wild-type LRRK2 (0.1 μM and 1 μM) were incubated with 10 μM of peptide either for 30 min at 20 °C or on ice overnight. Then, 500 μM GTP was added, and the production of GDP was monitored at 20 °C. To determine the amount of GDP and GTP, we used a reversed phase HPLC using a Hypersil Gold column (Thermofisher) with 10 mM tetra-n-butylammonium bromide, 50 mM phosphate buffer, and 14% ACN containing buffer. Data were integrated with Chromeleon 7 (Thermofisher) and fitted with Grafit 5 (Erithacus Software).

ROS Production Assay. Flow cytometry was used to measure reactive oxygen species (ROS) through fluorescence emission of the CellROX deep red dye (Life Technologies). RAW264.7 cells (ATCC SC-6003) were plated at 120 000/well in a 96-well low-adherence tissue culture plate (Costar). Cells were preincubated with stapled peptide or DMSO for 9 h then stimulated with Zymosan for 30 min (50 μg/mL). The CellROX staining was done according to the manufacturer's instructions; the CellROX reagent was added to the cell cultures at a final concentration of 2.5 μM, and the mixture was incubated for an additional 30 min. Cells were lifted, kept on ice, and analyzed immediately. Cells were then analyzed on Beckman Cytoflex flow cytometer (Beckman Coulter). The fluorescent channel was APC (638 nm excitation [ex], 660 nm emission [em]). Reported

https://doi.org/10.1021/acschembio.1c00487
ACS Chem. Biol. 2021, 16, 2326−2338

fluorescent intensity values represent arithmetic means of the results determined for analyzed cells.

Preparation of Primary Mouse Neuronal Cultures and Assessment of Neuronal Death. Embryonic day 16 (E16) pregnant C57BL mice were used in this study, with primary cortical neurons prepared as described.[70] Briefly, under aseptic conditions, cortices were removed and cut into small pieces before enzymatic digestion (trypsin 0.05% and 100 μg/mL DNase) and mechanical dissociation. Cells were centrifuged and counted and plated at a density of 150 000/cm^2 in BrainPhys neuronal culture medium (StemCell Technologies) supplemented with SM1 Neuronal Supplement (StemCell Technologies), L-glutamine (0.5 mM), and penicillin/streptavidin. After 3−4 DIV, neurons were transfected using Lipofectamine 2000 (Thermo Scientific) per the manufacturer's instructions. Neurons were transfected with Flag-tagged WT or mutant (G2019S) human LRRK2 (as described previously[70]). The following day, we initiated the treatment of neurons with fluorescently labeled peptides (at 10 μM final concentration). We replenished the peptides in the neuronal medium after 24 h and at the indicated concentrations. After 3 days following transfection, and 2 days of treatment, the coverslips were washed in PBS and fixed in 3.7% paraformaldehyde for 20 min at 4°C. The neurons were processed for immunofluorescence labeling with the following antibodies: GFP (chicken; Abcam), Flag (M2 mouse; Sigma-Aldrich), active caspase-3 (rabbit; R&D Systems), and DAPI nuclear stain. Mounted coverslips were imaged on a Leica TSP5 multiphoton confocal microscope and the Z-stacks processed in ImageJ and Adobe Photoshop. For quantification of apoptotic neuronal profiles, we used the approach described by Antoniou and colleagues.[70]

Statistical Analysis. GraphPad Prism was used for statistical analysis. One-way ANOVA and Dunnett's multiple comparisons test were used for the analysis of western blots and ROS production. n.s. = not significant, *p < 0.05, **p < 0.01, ***p < 0.001, and ****p < 0.0001. For neuronal apoptosis assay and *in vitro* dimerization assays, a one-way ANOVA with Tukey posthoc tests was performed. All experiments were performed in triplicate, at minimum. Unless otherwise stated, graphed data are presented as means ± SEM.

■ ASSOCIATED CONTENT

Supporting Information

The Supporting Information is available free of charge at https://pubs.acs.org/doi/10.1021/acschembio.1c00487.

Figure S1, circular dichroism of LCIP1; Figure S2, Co-IP identification of LCIP1 and LRIP4 as lead compounds; Figures S3 and S4, fluorescence polarization assays; Figure S5, quantification of LRRK2 dimerization; Figure S6, dose-dependent uptake of LCIP1 and LRIP4; Figures S7 and S8, proximity biotinylation assays; Figure S9, determination of heterodimer formation; Figure S10, G2019S overexpression model; Figure S11, Rab10 phosphorylation; Figure S12, GTPase assay; Figure S13, pS935-LRRK2 levels in cortical neurons; Figures S14−S21, ESI-mass spectrometry of all peptides (PDF)

Data for LRIP4 and LCIP1 (XLSX)

■ AUTHOR INFORMATION

Corresponding Authors

Arjan Kortholt − *Department of Cell Biochemistry, University of Groningen, 9747 Groningen, The Netherlands; Department of Pharmacology, Innovative Technologies Application and Research Center, Suleyman Demirel University, 32260 Isparta, Turkey*; Email: a.kortholt@rug.nl

Eileen J. Kennedy − *Department of Pharmaceutical and Biomedical Sciences, College of Pharmacy, University of Georgia, Athens, Georgia 30602, United States;* orcid.org/0000-0001-5610-1677; Email: ekennedy@uga.edu

Authors

Leah G. Helton − *Department of Pharmaceutical and Biomedical Sciences, College of Pharmacy, University of Georgia, Athens, Georgia 30602, United States*

Ahmed Soliman − *Department of Cell Biochemistry, University of Groningen, 9747 Groningen, The Netherlands;* orcid.org/0000-0003-2329-522X

Felix von Zweydorf − *DZNE, German Center for Neurodegenerative Diseases, 72076 Tübingen, Germany*

Michalis Kentros − *Center for Clinical, Experimental Surgery, and Translational Research, Biomedical Research Foundation of the Academy of Athens, 115 27 Athens, Greece*

Jascha T. Manschwetus − *Department of Biochemistry, Institute for Biology, University of Kassel, 34132 Kassel, Germany;* orcid.org/0000-0003-3136-9153

Scotty Hall − *Department of Pharmaceutical and Biomedical Sciences, College of Pharmacy, University of Georgia, Athens, Georgia 30602, United States*

Bernd Gilsbach − *DZNE, German Center for Neurodegenerative Diseases, 72076 Tübingen, Germany*

Franz Y. Ho − *Department of Cell Biochemistry, University of Groningen, 9747 Groningen, The Netherlands*

Panagiotis S. Athanasopoulos − *Department of Cell Biochemistry, University of Groningen, 9747 Groningen, The Netherlands*

Ranjan K. Singh − *VIB-VUB Center for Structural Biology, 1050 Brussels, Belgium; Structural Biology Brussels, Vrije Universiteit Brussel, 1050 Brussels, Belgium*

Timothy J. LeClair − *Department of Pharmaceutical and Biomedical Sciences, College of Pharmacy, University of Georgia, Athens, Georgia 30602, United States*

Wim Versées − *VIB-VUB Center for Structural Biology, 1050 Brussels, Belgium; Structural Biology Brussels, Vrije Universiteit Brussel, 1050 Brussels, Belgium*

Francesco Raimondi − *Laboratorio di Biologia Bio@SNS, Scuola Normale Superiore, 56126 Pisa, Italy*

Friedrich W. Herberg − *Department of Biochemistry, Institute for Biology, University of Kassel, 34132 Kassel, Germany;* orcid.org/0000-0001-7117-7653

Christian Johannes Gloeckner − *DZNE, German Center for Neurodegenerative Diseases, 72076 Tübingen, Germany; Core Facility for Medical Bioanalytics, Center for Ophthalmology, Institute for Ophthalmic Research, University of Tübingen, 72076 Tübingen, Germany*

Hardy Rideout − *Center for Clinical, Experimental Surgery, and Translational Research, Biomedical Research Foundation of the Academy of Athens, 115 27 Athens, Greece*

Complete contact information is available at: https://pubs.acs.org/10.1021/acschembio.1c00487

Author Contributions

[%]L.G.H. and A.S. are co-first authors.

Funding

The Michael J. Fox Foundation for Parkinson's Research has supported this work (8068.03, E.J.K., A.K., F.W.H, and C.J.G.; 8068.04, E.J.K., A.K., and C.J.G.; 11425.04, F.W.H.). A.K. is supported by a 2232 International Fellowship for Outstanding Researchers Program of TÜBİTAK (118C185). J.T.M. was supported by an Otto-Braun Predoctoral Fellowship (B. Braun Melsungen AG). W.V. was supported by the Fonds voor

Wetenschappelijk Onderzoek (FWO, G005219N) and Strategic Research Program Financing from the VUB (SRP50). H.J.R is supported by the Parkinson's Foundation and The Michael J. Fox Foundation for Parkinson's Research.

Notes

The authors declare no competing financial interest.

Author Contributions: L.G.H. and A.S. are co-first authors. L.G.H designed, synthesized, and characterized all stapled peptides with assistance from S.H. and T.J.L. under the guidance of E.J.K. Peptides were designed from a structural model developed by A.K., W.V., C.J.G., and F.R. L.G.H performed fluorescence polarization assays, serum stability assays, and circular dichroism. A.S. performed pull-downs, GFP trap dimerization experiments, flow cytometry, confocal imaging, ROS assay, and LRRK2 autophosphorylation assays with the assistance of P.S.A. under the guidance of A.K. J.T.M. performed protein purification and SPR analysis under the guidance of F.W.H. F.Y.H. purified proteins and performed the mass-spec experiments. Proximity biotinylation assays and neuronal apoptosis assays were performed by M.K. and H.R. R.S. performed binding assays under the guidance of W.V. Rab phosphorylation assays were performed by F.Z., and GTPase assays were performed by B.G. under the guidance of C.J.G. L.G.H. and A.S. wrote the manuscript with the help of all of the other authors.

REFERENCES

(1) Dorsey, E. R.; Constantinescu, R.; Thompson, J. P.; Biglan, K. M.; Holloway, R. G.; Kieburtz, K.; Marshall, F. J.; Ravina, B. M.; Schifitto, G.; Siderowf, A.; Tanner, C. M. Projected number of people with Parkinson disease in the most populous nations, 2005 through 2030. *Neurology* **2007**, *68*, 384−386.

(2) Dauer, W.; Przedborski, S. Parkinson's disease: mechanisms and models. *Neuron* **2003**, *39*, 889−909.

(3) Klein, C.; Westenberger, A. Genetics of Parkinson's disease. *Cold Spring Harbor Perspect. Med.* **2012**, *2*, a008888.

(4) Duvoisin, R. C. Recent advances in the genetics of Parkinson's disease. *Adv. Neurol* **1996**, *69*, 33−40.

(5) Polymeropoulos, M. H.; Lavedan, C.; Leroy, E.; Ide, S. E.; Dehejia, A.; Dutra, A.; Pike, B.; Root, H.; Rubenstein, J.; Boyer, R.; Stenroos, E. S.; Chandrasekharappa, S.; Athanassiadou, A.; Papapetropoulos, T.; Johnson, W. G.; Lazzarini, A. M.; Duvoisin, R. C.; Di Iorio, G.; Golbe, L. I.; Nussbaum, R. L. Mutation in the alpha-synuclein gene identified in families with Parkinson's disease. *Science* **1997**, *276*, 2045−2047.

(6) Kruger, R.; Kuhn, W.; Muller, T.; Woitalla, D.; Graeber, M.; Kosel, S.; Przuntek, H.; Epplen, J. T.; Schols, L.; Riess, O. Ala30Pro mutation in the gene encoding alpha-synuclein in Parkinson's disease. *Nat. Genet.* **1998**, *18*, 106−108.

(7) Farrer, M.; Gwinn-Hardy, K.; Muenter, M.; DeVrieze, F. W.; Crook, R.; Perez-Tur, J.; Lincoln, S.; Maraganore, D.; Adler, C.; Newman, S.; MacElwee, K.; McCarthy, P.; Miller, C.; Waters, C.; Hardy, J. A chromosome 4p haplotype segregating with Parkinson's disease and postural tremor. *Hum. Mol. Genet.* **1999**, *8*, 81−85.

(8) Gasser, T.; Muller-Myhsok, B.; Wszolek, Z. K.; Oehlmann, R.; Calne, D. B.; Bonifati, V.; Bereznai, B.; Fabrizio, E.; Vieregge, P.; Horstmann, R. D. A susceptibility locus for Parkinson's disease maps to chromosome 2p13. *Nat. Genet.* **1998**, *18*, 262−265.

(9) Gasser, T. Mendelian forms of Parkinson's disease. *Biochim. Biophys. Acta, Mol. Basis Dis.* **2009**, *1792*, 587−596.

(10) Zimprich, A.; Biskup, S.; Leitner, P.; Lichtner, P.; Farrer, M.; Lincoln, S.; Kachergus, J.; Hulihan, M.; Uitti, R. J.; Calne, D. B.; Stoessl, A. J.; Pfeiffer, R. F.; Patenge, N.; Carbajal, I. C.; Vieregge, P.; Asmus, F.; Muller-Myhsok, B.; Dickson, D. W.; Meitinger, T.; Strom, T. M.; Wszolek, Z. K.; Gasser, T. Mutations in LRRK2 cause autosomal-dominant parkinsonism with pleomorphic pathology. *Neuron* **2004**, *44*, 601−607.

(11) Verstraeten, A.; Theuns, J.; Van Broeckhoven, C. Progress in unraveling the genetic etiology of Parkinson disease in a genomic era. *Trends Genet.* **2015**, *31*, 140−149.

(12) Biosa, A.; Trancikova, A.; Civiero, L.; Glauser, L.; Bubacco, L.; Greggio, E.; Moore, D. J. GTPase activity regulates kinase activity and cellular phenotypes of Parkinson's disease-associated LRRK2. *Hum. Mol. Genet.* **2013**, *22*, 1140−1156.

(13) Mata, I. F.; Wedemeyer, W. J.; Farrer, M. J.; Taylor, J. P.; Gallo, K. A. LRRK2 in Parkinson's disease: protein domains and functional insights. *Trends Neurosci.* **2006**, *29*, 286−293.

(14) Li, J. Q.; Tan, L.; Yu, J. T. The role of the LRRK2 gene in Parkinsonism. *Mol. Neurodegener.* **2014**, *9*, 47.

(15) Tolosa, E.; Vila, M.; Klein, C.; Rascol, O. LRRK2 in Parkinson disease: challenges of clinical trials. *Nat. Rev. Neurol.* **2020**, *16*, 97.

(16) Simon-Sanchez, J.; Schulte, C.; Bras, J. M.; Sharma, M.; Gibbs, J. R.; Berg, D.; Paisan-Ruiz, C.; Lichtner, P.; Scholz, S. W.; Hernandez, D. G.; Kruger, R.; Federoff, M.; Klein, C.; Goate, A.; Perlmutter, J.; Bonin, M.; Nalls, M. A.; Illig, T.; Gieger, C.; Houlden, H.; Steffens, M.; Okun, M. S.; Racette, B. A.; Cookson, M. R.; Foote, K. D.; Fernandez, H. H.; Traynor, B. J.; Schreiber, S.; Arepalli, S.; Zonozi, R.; Gwinn, K.; van der Brug, M.; Lopez, G.; Chanock, S. J.; Schatzkin, A.; Park, Y.; Hollenbeck, A.; Gao, J.; Huang, X.; Wood, N. W.; Lorenz, D.; Deuschl, G.; Chen, H.; Riess, O.; Hardy, J. A.; Singleton, A. B.; Gasser, T. Genome-wide association study reveals genetic risk underlying Parkinson's disease. *Nat. Genet.* **2009**, *41*, 1308−1312.

(17) Di Maio, R.; Hoffman, E. K.; Rocha, E. M.; Keeney, M. T.; Sanders, L. H.; De Miranda, B. R.; Zharikov, A.; Van Laar, A.; Stepan, A. F.; Lanz, T. A.; Kofler, J. K.; Burton, E. A.; Alessi, D. R.; Hastings, T. G.; Greenamyre, J. T. LRRK2 activation in idiopathic Parkinson's disease. *Sci. Transl. Med.* **2018**, *10*, eaar5429.

(18) Deng, X.; Choi, H. G.; Buhrlage, S. J.; Gray, N. S. Leucine-rich repeat kinase 2 inhibitors: a patent review (2006 - 2011). *Expert Opin. Ther. Pat.* **2012**, *22*, 1415−1426.

(19) Fuji, R. N.; Flagella, M.; Baca, M.; Baptista, M. A.; Brodbeck, J.; Chan, B. K.; Fiske, B. K.; Honigberg, L.; Jubb, A. M.; Katavolos, P.; Lee, D. W.; Lewin-Koh, S. C.; Lin, T.; Liu, X.; Liu, S.; Lyssikatos, J. P.; O'Mahony, J.; Reichelt, M.; Roose-Girma, M.; Sheng, Z.; Sherer, T.; Smith, A.; Solon, M.; Sweeney, Z. K.; Tarrant, J.; Urkowitz, A.; Warming, S.; Yaylaoglu, M.; Zhang, S.; Zhu, H.; Estrada, A. A.; Watts, R. J. Effect of selective LRRK2 kinase inhibition on nonhuman primate lung. *Sci. Transl. Med.* **2015**, *7*, 273ra15.

(20) Berger, Z.; Smith, K. A.; Lavoie, M. J. Membrane localization of LRRK2 is associated with increased formation of the highly active LRRK2 dimer and changes in its phosphorylation. *Biochemistry* **2010**, *49*, 5511−5523.

(21) James, N. G.; Digman, M. A.; Gratton, E.; Barylko, B.; Ding, X.; Albanesi, J. P.; Goldberg, M. S.; Jameson, D. M. Number and brightness analysis of LRRK2 oligomerization in live cells. *Biophys. J.* **2012**, *102*, L41−43.

(22) Greggio, E.; Zambrano, I.; Kaganovich, A.; Beilina, A.; Taymans, J. M.; Daniels, V.; Lewis, P.; Jain, S.; Ding, J.; Syed, A.; Thomas, K. J.; Baekelandt, V.; Cookson, M. R. The Parkinson disease-associated leucine-rich repeat kinase 2 (LRRK2) is a dimer that undergoes intramolecular autophosphorylation. *J. Biol. Chem.* **2008**, *283*, 16906−16914.

(23) Nichols, W. C.; Pankratz, N.; Hernandez, D.; Paisan-Ruiz, C.; Jain, S.; Halter, C. A.; Michaels, V. E.; Reed, T.; Rudolph, A.; Shults, C. W.; Singleton, A.; Foroud, T.; Parkinson Study Group, P. i.. Genetic screening for a single common LRRK2 mutation in familial Parkinson's disease. *Lancet* **2005**, *365*, 410−412.

(24) Kachergus, J.; Mata, I. F.; Hulihan, M.; Taylor, J. P.; Lincoln, S.; Aasly, J.; Gibson, J. M.; Ross, O. A.; Lynch, T.; Wiley, J.; Payami, H.; Nutt, J.; Maraganore, D. M.; Czyzewski, K.; Styczynska, M.; Wszolek, Z. K.; Farrer, M. J.; Toft, M. Identification of a novel LRRK2 mutation linked to autosomal dominant parkinsonism: evidence of a

https://doi.org/10.1021/acschembio.1c00487
ACS Chem. Biol. 2021, 16, 2326−2338

common founder across European populations. *Am. J. Hum. Genet.* **2005**, *76*, 672−680.
(25) Bonifati, V. Parkinson's disease: the LRRK2-G2019S mutation: opening a novel era in Parkinson's disease genetics. *Eur. J. Hum. Genet.* **2006**, *14*, 1061−1062.
(26) West, A. B.; Moore, D. J.; Biskup, S.; Bugayenko, A.; Smith, W. W.; Ross, C. A.; Dawson, V. L.; Dawson, T. M. Parkinson's disease-associated mutations in leucine-rich repeat kinase 2 augment kinase activity. *Proc. Natl. Acad. Sci. U. S. A.* **2005**, *102*, 16842−16847.
(27) Watanabe, R.; Buschauer, R.; Bohning, J.; Audagnotto, M.; Lasker, K.; Lu, T. W.; Boassa, D.; Taylor, S.; Villa, E. The In Situ Structure of Parkinson's Disease-Linked LRRK2. *Cell* **2020**, *182*, 1508.
(28) Deniston, C. K.; Salogiannis, J.; Mathea, S.; Snead, D. M.; Lahiri, I.; Matyszewski, M.; Donosa, O.; Watanabe, R.; Bohning, J.; Shiau, A. K.; Knapp, S.; Villa, E.; Reck-Peterson, S. L.; Leschziner, A. E. Structure of LRRK2 in Parkinson's disease and model for microtubule interaction. *Nature* **2020**, *588*, 895367.
(29) Myasnikov, A.; Zhu, H.; Hixson, P.; Xie, B.; Yu, K.; Pitre, A.; Peng, J.; Sun, J. Structural analysis of the full-length human LRRK2. *Cell* **2021**, *184*, 3519.
(30) Schmidt, S. H.; Aoto, P. C.; Boassa, D.; Mathea, S.; Silletti, S.; Hu, J.; Wallbott, M.; Komives, E. A.; Knapp, S.; Herberg, F. W.; Taylor, S. S. Conformation and dynamics of the kinase domain drive subcellular location and activation of LRRK2. *bioRxiv*, **2020**.
(31) Taylor, S. S.; Kaila-Sharma, P.; Weng, J. H.; Aoto, P.; Schmidt, S. H.; Knapp, S.; Mathea, S.; Herberg, F. W. Kinase Domain Is a Dynamic Hub for Driving LRRK2 Allostery. *Front. Mol. Neurosci.* **2020**, *13*, 538219.
(32) Verdine, G. L.; Hilinski, G. J. Stapled peptides for intracellular drug targets. *Methods Enzymol.* **2012**, *503*, 3−33.
(33) Helton, L. G.; Kennedy, E. J. Targeting Plasmodium with constrained peptides and peptidomimetics. *IUBMB Life* **2020**, *72*, 1103−1114.
(34) Bendzunas, N. G.; Dorfler, S.; Autenrieth, K.; Bertinetti, D.; Machal, E. M. F.; Kennedy, E. J.; Herberg, F. W. Investigating PKA-RII specificity using analogs of the PKA:AKAP peptide inhibitor STAD-2. *Bioorg. Med. Chem.* **2018**, *26*, 1174−1178.
(35) Manschwetus, J. T.; Bendzunas, G. N.; Limaye, A. J.; Knape, M. J.; Herberg, F. W.; Kennedy, E. J. A Stapled Peptide Mimic of the Pseudosubstrate Inhibitor PKI Inhibits Protein Kinase A. *Molecules* **2019**, *24*, 1567.
(36) Cowell, J. K.; Teng, Y.; Bendzunas, N. G.; Ara, R.; Arbab, A. S.; Kennedy, E. J. Suppression of Breast Cancer Metastasis Using Stapled Peptides Targeting the WASF Regulatory Complex. *Cancer Growth Metastasis* **2017**, *10*, 117906441771319.
(37) Fulton, M. D.; Hanold, L. E.; Ruan, Z.; Patel, S.; Beedle, A. M.; Kannan, N.; Kennedy, E. J. Conformationally constrained peptides target the allosteric kinase dimer interface and inhibit EGFR activation. *Bioorg. Med. Chem.* **2018**, *26*, 1167−1173.
(38) Hanold, L. E.; Fulton, M. D.; Kennedy, E. J. Targeting kinase signaling pathways with constrained peptide scaffolds. *Pharmacol. Ther.* **2017**, *173*, 159−170.
(39) Gilsbach, B. K.; Ho, F. Y.; Vetter, I. R.; van Haastert, P. J.; Wittinghofer, A.; Kortholt, A. Roco kinase structures give insights into the mechanism of Parkinson disease-related leucine-rich-repeat kinase 2 mutations. *Proc. Natl. Acad. Sci. U. S. A.* **2012**, *109*, 10322−10327.
(40) Deyaert, E.; Leemans, M.; Singh, R. K.; Gallardo, R.; Steyaert, J.; Kortholt, A.; Lauer, J.; Versees, W. Structure and nucleotide-induced conformational dynamics of the Chlorobium tepidum Roco protein. *Biochem. J.* **2019**, *476*, 51−66.
(41) Deyaert, E.; Wauters, L.; Guaitoli, G.; Konijnenberg, A.; Leemans, M.; Terheyden, S.; Petrovic, A.; Gallardo, R.; Nederveen-Schippers, L. M.; Athanasopoulos, P. S.; Pots, H.; Van Haastert, P. J. M.; Sobott, F.; Gloeckner, C. J.; Efremov, R.; Kortholt, A.; Versees, W. A homologue of the Parkinson's disease-associated protein LRRK2 undergoes a monomer-dimer transition during GTP turnover. *Nat. Commun.* **2017**, *8*, 1008.
(42) Nguyen, A. P.; Moore, D. J. Understanding the GTPase Activity of LRRK2: Regulation, Function, and Neurotoxicity. *Adv. Neurobiol* **2017**, *14*, 71−88.
(43) Wu, C. X.; Liao, J.; Park, Y.; Reed, X.; Engel, V. A.; Hoang, N. C.; Takagi, Y.; Johnson, S. M.; Wang, M.; Federici, M.; Nichols, R. J.; Sanishvili, R.; Cookson, M. R.; Hoang, Q. Q. Parkinson's disease-associated mutations in the GTPase domain of LRRK2 impair its nucleotide-dependent conformational dynamics. *J. Biol. Chem.* **2019**, *294*, 5907−5913.
(44) Guaitoli, G.; Raimondi, F.; Gilsbach, B. K.; Gómez-Llorente, Y.; Deyaert, E.; Renzi, F.; Li, X.; Schaffner, A.; Jagtap, P. K. A.; Boldt, K.; von Zweydorf, F.; Gotthardt, K.; Lorimer, D. D.; Yue, Z.; Burgin, A.; Janjic, N.; Sattler, M.; Versées, W.; Ueffing, M.; Ubarretxena-Belandia, I.; Kortholt, A.; Gloeckner, C. J. Structural model of the dimeric Parkinson's protein LRRK2 reveals a compact architecture involving distant interdomain contacts. *Proc. Natl. Acad. Sci. U. S. A.* **2016**, *113*, E4357.
(45) Blackwell, H. E.; Grubbs, R. H. Highly Efficient Synthesis of Covalently Cross-Linked Peptide Helices by Ring-Closing Metathesis. *Angew. Chem., Int. Ed.* **1998**, *37*, 3281−3284.
(46) Leandrou, E.; Markidi, E.; Memou, A.; Melachroinou, K.; Greggio, E.; Rideout, H. J. Kinase activity of mutant LRRK2 manifests differently in hetero-dimeric vs. homo-dimeric complexes. *Biochem. J.* **2019**, *476*, 559−579.
(47) Sheng, Z.; Zhang, S.; Bustos, D.; Kleinheinz, T.; Le Pichon, C. E.; Dominguez, S. L.; Solanoy, H. O.; Drummond, J.; Zhang, X.; Ding, X.; Cai, F.; Song, Q.; Li, X.; Yue, Z.; van der Brug, M. P.; Burdick, D. J.; Gunzner-Toste, J.; Chen, H.; Liu, X.; Estrada, A. A.; Sweeney, Z. K.; Scearce-Levie, K.; Moffat, J. G.; Kirkpatrick, D. S.; Zhu, H. Ser1292 autophosphorylation is an indicator of LRRK2 kinase activity and contributes to the cellular effects of PD mutations. *Sci. Transl. Med.* **2012**, *4*, 164ra161.
(48) Steger, M.; Tonelli, F.; Ito, G.; Davies, P.; Trost, M.; Vetter, M.; Wachter, S.; Lorentzen, E.; Duddy, G.; Wilson, S.; Baptista, M. A.; Fiske, B. K.; Fell, M. J.; Morrow, J. A.; Reith, A. D.; Alessi, D. R.; Mann, M. Phosphoproteomics reveals that Parkinson's disease kinase LRRK2 regulates a subset of Rab GTPases. *eLife* **2016**, *5*, e12813.
(49) Yin, G.; Lopes da Fonseca, T.; Eisbach, S. E.; Anduaga, A. M.; Breda, C.; Orcellet, M. L.; Szego, E. M.; Guerreiro, P.; Lazaro, D. F.; Braus, G. H.; Fernandez, C. O.; Griesinger, C.; Becker, S.; Goody, R. S.; Itzen, A.; Giorgini, F.; Outeiro, T. F.; Zweckstetter, M. alpha-Synuclein interacts with the switch region of Rab8a in a Ser129 phosphorylation-dependent manner. *Neurobiol. Dis.* **2014**, *70*, 149−161.
(50) Liu, Z.; Bryant, N.; Kumaran, R.; Beilina, A.; Abeliovich, A.; Cookson, M. R.; West, A. B. LRRK2 phosphorylates membrane-bound Rabs and is activated by GTP-bound Rab7L1 to promote recruitment to the trans-Golgi network. *Hum. Mol. Genet.* **2018**, *27*, 385−395.
(51) Purlyte, E.; Dhekne, H. S.; Sarhan, A. R.; Gomez, R.; Lis, P.; Wightman, M.; Martinez, T. N.; Tonelli, F.; Pfeffer, S. R.; Alessi, D. R. Rab29 activation of the Parkinson's disease-associated LRRK2 kinase. *EMBO J.* **2018**, *37*, 1−18.
(52) Kett, L. R.; Boassa, D.; Ho, C. C.; Rideout, H. J.; Hu, J.; Terada, M.; Ellisman, M.; Dauer, W. T. LRRK2 Parkinson disease mutations enhance its microtubule association. *Hum. Mol. Genet.* **2012**, *21*, 890−899.
(53) Berwick, D. C.; Heaton, G. R.; Azeggagh, S.; Harvey, K. LRRK2 Biology from structure to dysfunction: research progresses, but the themes remain the same. *Mol. Neurodegener.* **2019**, *14*, 49.
(54) Saez-Atienzar, S.; Bonet-Ponce, L.; Blesa, J. R.; Romero, F. J.; Murphy, M. P.; Jordan, J.; Galindo, M. F. The LRRK2 inhibitor GSK2578215A induces protective autophagy in SH-SY5Y cells: involvement of Drp-1-mediated mitochondrial fission and mitochondrial-derived ROS signaling. *Cell Death Dis.* **2014**, *5*, e1368.
(55) Heo, H. Y.; Park, J.-M.; Kim, C.-H.; Han, B. S.; Kim, K.-S.; Seol, W. LRRK2 enhances oxidative stress-induced neurotoxicity via its kinase activity. *Exp. Cell Res.* **2010**, *316*, 649−656.

https://doi.org/10.1021/acschembio.1c00487
ACS Chem. Biol. 2021, 16, 2326−2338

(56) Kim, J.; Pajarillo, E.; Rizor, A.; Son, D. S.; Lee, J.; Aschner, M.; Lee, E. LRRK2 kinase plays a critical role in manganese-induced inflammation and apoptosis in microglia. *PLoS One* **2019**, *14*, e0210248.
(57) Gardet, A.; Benita, Y.; Li, C.; Sands, B. E.; Ballester, I.; Stevens, C.; Korzenik, J. R.; Rioux, J. D.; Daly, M. J.; Xavier, R. J.; Podolsky, D. K. LRRK2 Is Involved in the IFN-γ Response and Host Response to Pathogens. *J. Immunol.* **2010**, *185*, 5577.
(58) Nguyen, A. P. T.; Tsika, E.; Kelly, K.; Levine, N.; Chen, X.; West, A. B.; Boularand, S.; Barneoud, P.; Moore, D. J. Dopaminergic neurodegeneration induced by Parkinson's disease-linked G2019S LRRK2 is dependent on kinase and GTPase activity. *Proc. Natl. Acad. Sci. U. S. A.* **2020**, *117*, 17296−17307.
(59) Skibinski, G.; Nakamura, K.; Cookson, M. R.; Finkbeiner, S. Mutant LRRK2 toxicity in neurons depends on LRRK2 levels and synuclein but not kinase activity or inclusion bodies. *J. Neurosci.* **2014**, *34*, 418−433.
(60) Herzig, M. C.; Kolly, C.; Persohn, E.; Theil, D.; Schweizer, T.; Hafner, T.; Stemmelen, C.; Troxler, T. J.; Schmid, P.; Danner, S.; Schnell, C. R.; Mueller, M.; Kinzel, B.; Grevot, A.; Bolognani, F.; Stirn, M.; Kuhn, R. R.; Kaupmann, K.; van der Putten, P. H.; Rovelli, G.; Shimshek, D. R. LRRK2 protein levels are determined by kinase function and are crucial for kidney and lung homeostasis in mice. *Hum. Mol. Genet.* **2011**, *20*, 4209−4223.
(61) Baptista, M. A.; Dave, K. D.; Frasier, M. A.; Sherer, T. B.; Greeley, M.; Beck, M. J.; Varsho, J. S.; Parker, G. A.; Moore, C.; Churchill, M. J.; Meshul, C. K.; Fiske, B. K. Loss of leucine-rich repeat kinase 2 (LRRK2) in rats leads to progressive abnormal phenotypes in peripheral organs. *PLoS One* **2013**, *8*, e80705.
(62) Sen, S.; Webber, P. J.; West, A. B. Dependence of leucine-rich repeat kinase 2 (LRRK2) kinase activity on dimerization. *J. Biol. Chem.* **2009**, *284*, 36346−36356.
(63) Berger, Z.; Smith, K. A.; LaVoie, M. J. Membrane Localization of LRRK2 Is Associated with Increased Formation of the Highly Active LRRK2 Dimer and Changes in Its Phosphorylation. *Biochemistry* **2010**, *49*, 5511−5523.
(64) Greggio, E.; Zambrano, I.; Kaganovich, A.; Beilina, A.; Taymans, J.-M.; Daniëls, V.; Lewis, P.; Jain, S.; Ding, J.; Syed, A.; Thomas, K. J.; Baekelandt, V.; Cookson, M. R. The Parkinson Disease-associated Leucine-rich Repeat Kinase 2 (LRRK2) Is a Dimer That Undergoes Intramolecular Autophosphorylation. *J. Biol. Chem.* **2008**, *283*, 16906−16914.
(65) Daniëls, V.; Vancraenenbroeck, R.; Law, B. M. H.; Greggio, E.; Lobbestael, E.; Gao, F.; De Maeyer, M.; Cookson, M. R.; Harvey, K.; Baekelandt, V.; Taymans, J.-M. Insight into the mode of action of the LRRK2 Y1699C pathogenic mutant. *J. Neurochem.* **2011**, *116*, 304−315.
(66) Civiero, L.; Vancraenenbroeck, R.; Belluzzi, E.; Beilina, A.; Lobbestael, E.; Reyniers, L.; Gao, F.; Micetic, I.; De Maeyer, M.; Bubacco, L.; Baekelandt, V.; Cookson, M. R.; Greggio, E.; Taymans, J.-M. Biochemical Characterization of Highly Purified Leucine-Rich Repeat Kinases 1 and 2 Demonstrates Formation of Homodimers. *PLoS One* **2012**, *7*, e43472.
(67) Leemans, M.; Galicia, C.; Deyaert, E.; Daems, E.; Krause, L.; Paesmans, J.; Pardon, E.; Steyaert, J.; Kortholt, A.; Sobott, F.; Klostermeier, D.; Versees, W. Allosteric modulation of the GTPase activity of a bacterial LRRK2 homolog by conformation-specific Nanobodies. *Biochem. J.* **2020**, *477*, 1203−1218.
(68) Carrion, M. D. P.; Marsicano, S.; Daniele, F.; Marte, A.; Pischedda, F.; Di Cairano, E.; Piovesana, E.; von Zweydorf, F.; Kremmer, E.; Gloeckner, C. J.; Onofri, F.; Perego, C.; Piccoli, G. The LRRK2 G2385R variant is a partial loss-of-function mutation that affects synaptic vesicle trafficking through altered protein interactions. *Sci. Rep.* **2017**, *7*, 5377.
(69) Fernandez-Suarez, M.; Chen, T. S.; Ting, A. Y. Protein-protein interaction detection in vitro and in cells by proximity biotinylation. *J. Am. Chem. Soc.* **2008**, *130*, 9251−9253.
(70) Antoniou, N.; Vlachakis, D.; Memou, A.; Leandrou, E.; Valkimadi, P. E.; Melachroinou, K.; Re, D. B.; Przedborski, S.; Dauer, W. T.; Stefanis, L.; Rideout, H. J. A motif within the armadillo repeat of Parkinson's-linked LRRK2 interacts with FADD to hijack the extrinsic death pathway. *Sci. Rep.* **2018**, *8*, 3455.

https://doi.org/10.1021/acschembio.1c00487
ACS Chem. Biol. 2021, 16, 2326−2338